A 3D Reactive Collision Avoidance Algorithm for Underactuated Vehicles

Martin S. Wiig[1,2], Kristin Y. Pettersen[1,2] and Thomas R. Krogstad[2]

***Abstract*— This paper presents a 3D reactive collision avoidance algorithm for vehicles with underactuated dynamics. The underactuated states cannot be directly controlled, but are controlled indirectly by steering the direction of the vehicle's velocity vector. This vector is made to point a constant avoidance angle away from the obstacle, thus ensuring collision avoidance, while the forward speed is kept constant to maintain maneuverability. We choose an optimal pair of desired heading and pitch angles during the maneuver, thus taking advantage of the flexibility provided by operating in 3D. The algorithm incorporates limits on both the allowed pitch angle and the control inputs, which are limits that often are present in practical scenarios. Finally, we provide a mathematical proof that the collision avoidance maneuver is safe, and support the analysis through several simulations.**

I. INTRODUCTION

Unmanned vehicles often operate in unknown and dynamic environments with little or no manned supervision. In such scenarios, it is of vital importance that the vehicle is able to avoid collisions with any obstacles it encounters. Collision avoidance can become particularly demanding for underactuated vehicles, such as most autonomous underwater vehicles (AUVs), as not all degrees of freedom can be controlled independently. The underactuation will generally introduce second-order nonholonomic constraints, which make it necessary to consider the underactuated dynamics [1] in the analysis and control design of such vehicles.

There are several existing collision avoidance (CA) algorithms [2]–[4], particularly in 2D. The different approaches can be divided into reactive algorithms and motion planning algorithms. Motion planning for vehicles with complex dynamics operating in dynamic environments can be too expensive for vehicles with limited processing power, particularly in 3D which has significantly added computational complexity. This necessitates the use of reactive algorithms.

The family of artificial potential field algorithms [5]–[7] is a much used approach to CA, and can be intuitively interpreded and easily extended. There is, however, an underlying assumption that the vehicle is always able to follow the gradient of the field, and neither nonholonomic constraints nor vehicle dynamics tend to be considered in the analysis.

This work was partly supported by the Research Council of Norway through the Centres of Excellence funding scheme, project no. 223254 - NTNU AMOS

[1]Centre for Autonomous Marine Operations and Systems (NTNU AMOS), Department of Engineering Cybernetics, Norwegian University of Science and Technology, 7491 Trondheim, Norway. Martin.Wiig@ntnu.no

[2]Norwegian Defence Research Establishment (FFI), P.O. Box 25, N-2027 Kjeller, Norway.

The dynamic window algorithm [8] considers vehicle dynamics and constraints by searching through a set of valid trajectories to find an optimal control output, and is extended to an underactuated vehicle in [9]. However, since the algorithm is based on a computational search through a set of generated trajectories, it can become intractable in 3D.

The velocity obstacle [10] and collision cone [11] approaches are equivalent algorithms for avoiding several moving obstacles in the plane. The velocity obstacle approach has been extended to include acceleration constraints and nonholonomic constraints [12], [13], and has been used with much success. However, for vehicles with very limited speed envelopes, it can become too restrictive.

The problem of finding a safe velocity in 3D is elegantly solved in [14] and [15], which extend velocity obstacles to 3D by dividing the 3D space into a discrete set of planes. The vehicle can then choose the best safe velocity among the multiple planes. Vehicle dynamics are, however, not considered, and there is a possibility of oscillations when switching between different avoidance planes.

In [16], the collision cone framework is used to make a system of 3D vehicles remain provably collision free if it starts in a conflict-free state. The result is very strong and general, and incorporates speed and acceleration constraints. However, while the vehicle's dynamics are implicitly included using a robustness analysis, they are not explicitly accounted for. Furthermore, the deconfliction algorithm for vehicles on a collision course is in 2D.

The algorithm presented by [17] makes the vehicle avoid a moving obstacle by keeping a constant avoidance angle to it. The kinematic vehicle model incorporates nonholonomic constraints, and avoidance is mathematically proved. However, the algorithm can require significant forward acceleration of the vehicle, and can make it almost stop. This is unfortunate for example for many marine vehicles, which loses maneuverability at low speed and spends much energy during forward acceleration. Furthermore, the algorithm has a singularity for some obstacle speeds.

In [18] the algorithm in [17] is extended to 3D by creating a plane using the vehicle's velocity vector and the obstacle center, and then employing the 2D algorithm in this plane. This is an intuitive extension, and it is again proved that the algorithm is safe. However, the algorithm suffers from the same problems as [17], and does not fully make use of the flexibility offered by operating in 3D.

The algorithm proposed in [19] extends the work of [17] to accommodate vehicles that must move within a limited speed envelope, and removes the singularity. Specifically,

the algorithm makes the vehicle provably avoid obstacles by steering the vehicle heading, leaving the forward speed to be freely designed to accommodate other objectives. This feature is utilized in [20], where the algorithm is extended to a marine 2D vehicle with underactuated dynamics. When such a vehicle turns, a sideways speed is induced, which can drive the vehicle towards the obstacle. Thus, a purely kinematic model cannot be employed for control design and analysis. In [20], this is solved by steering the direction of the vehicle's velocity vector. Actuator constraints are, however, not directly incorporated in the analysis.

In [21], the algorithm of [19] is extended to 3D collision avoidance for nonholonomic vehicles by introducing a 3D vision cone from the vehicle to the obstacle. The vision cone is extended by a constant avoidance angle, and the vehicle will follow one of the rays of this extended vision cone in order to avoid the obstacle. The algorithm makes use of the flexibility offered by moving in 3D, and in particular chooses an optimal pair of desired heading and pitch to avoid the obstacle using minimum control effort. Furthermore, the algorithm can incorporate vehicle pitch limitations, which is often an important safety feature of vehicles operating in 3D.

The main contribution of this paper is an extension of the 3D algorithm in [21] to underactuated marine vehicles. Such vehicles have underactuated sway and heave dynamics, which can only be indirectly controlled through the actuated states. Like in [20], these underactuated dynamics need to be considered in the control design and analysis, preventing the use of the purely kinematic model used in [21]. In this paper, we will steer the direction of the vehicle's velocity vector in 3D, which is not straightforward due to the presence of composite rotations. Specifically, we derive a method for converting a desired angular velocity of the vehicle velocity vector into control inputs of the vehicle, while maintaining actuator constraints. Furthermore, we show that the sway and heave dynamics are bounded during the maneuver, and we show how to include constraints in the controllers. Finally, we derive conditions under which it is mathematically proved that the obstacle will be avoided while keeping a constant surge speed and upholding limits on the pitch of the velocity vector.

The remainder of this paper is organized as follows. Some mathematical definitions are presented in Section II, while the vehicle model is presented in Section III, which also states the sensor requirements and the control objective of the system. Section IV states the controllers for the direction of the velocity vector, as well as the guidance laws employed to steer the vehicle towards a target when it is not in CA mode. Section V describes the CA algorithm, which is analyzed in Section VI. The analysis is validated by simulations in Section VII. Finally, concluding remarks and thoughts on future work are given in Section VIII.

II. MATHEMATICAL PRELIMINARIES

The trigonometric functions $\sin(\cdot)$, $\cos(\cdot)$ and $\tan(\cdot)$ will be denoted $s(\cdot)$, $c(\cdot)$ and $t(\cdot)$, respectively.

A point p and vector $\boldsymbol{v}$ in a reference frame a are denoted p^a and $\boldsymbol{v}^a$, respectively. The rotation matrix from reference frame a to a frame b is denoted $\boldsymbol{R}_a^b$, so that $\boldsymbol{v}^b = \boldsymbol{R}_a^b \boldsymbol{v}^a$.

The rotation matrix $\boldsymbol{R}_{zyx}(\varphi, \theta, \psi)$ represents a composite rotation using the zyx convention, and we define $\boldsymbol{R}_{zy}(\theta, \psi) \triangleq \boldsymbol{R}_{zyx}(0, \theta, \psi)$ and $\boldsymbol{R}_z(\psi) \triangleq \boldsymbol{R}_{zyx}(0, 0, \psi)$.

We define the following functions converting the vector $\boldsymbol{v} = [v_x, v_y, v_z]^T$ into a heading and pitch angle:

$$\Psi(\boldsymbol{v}) = \operatorname{atan2}(v_y, v_x), \tag{1}$$

$$\Theta(\boldsymbol{v}) = -\sin^{-1}\left(\tfrac{v_z}{||\boldsymbol{v}||}\right). \tag{2}$$

III. SYSTEM DESCRIPTION

A. Vehicle model

The vehicle is modeled in 5 degrees of freedom using the Euler angles yaw (ψ_v) and pitch (θ_v) to transform the vehicle velocity from the Body frame b to the North-east-down (NED) frame n.

Assumption 1: The vehicle is passively stabilized in roll.

The vehicle is directly actuated in surge u_v, yaw r_v and pitch q_v, but has no actuation in sway v_v and heave w_v. Hence, the sway and heave dynamics have to be included in the model, while the surge, yaw and pitch dynamics can be removed by Assumption 2.

Assumption 2: The Body-fixed surge speed u_v and angular velocities in yaw, r_v, and pitch, q_v, are assumed to be directly controlled. The surge speed is kept constant, while

$$r_v \in [-r_{v\max}, r_{v\max}], \tag{3a}$$

$$q_v \in [-q_{v\max}, q_{v\max}], \tag{3b}$$

where $r_{v\max} > 0$ and $q_{v\max} > 0$ are constant parameters.

The vehicle model is then:

$$\dot{\boldsymbol{p}}_{\mathrm{v}}^n = \boldsymbol{R}_{zy}(\theta_v, \psi_v)\boldsymbol{\nu}_{\mathrm{v}}^b, \tag{4a}$$

$$\dot{\theta}_v = q_v, \tag{4b}$$

$$\dot{\psi}_v = \tfrac{r_v}{\cos(\theta_v)}, \tag{4c}$$

$$\dot{v}_v = X_v r_v + Y_v v_v, \tag{4d}$$

$$\dot{w}_v = X_w q_v + Y_w w_v + Z_w \sin(\theta_v), \tag{4e}$$

where $\boldsymbol{p}_{\mathrm{v}}^n$ is the vehicle position in the NED frame and $\boldsymbol{\nu}_{\mathrm{v}}^b = [u_v, v_v, w_v]^T$, i.e. the surge, sway and heave speed of the vehicle, respectively. The parameters X_v, Y_v, X_w, Y_w and Z_w are constants derived from the mass and damping parameters of the vehicle [22], [23].

To ensure that the vehicle is nominally stable in sway and heave, we make the following assumption:

Assumption 3: The parameters Y_v and Y_w are negative.

This assumption holds for most marine vehicles by design.

We also define a Body-fixed reference frame n_v, which is oriented along the NED frame, which is useful for representing positions relative to the vehicle.

B. The Flow frame

To avoid an obstacle we will steer the vehicle's velocity vector. To this end, we represent the vehicle model (4) in the Flow frame f [22], such that $\dot{\boldsymbol{p}}_{\mathrm{v}}^n = \boldsymbol{R}_f^n(\theta_v, \psi_v)\boldsymbol{\nu}_{\mathrm{v}}^f$,

where $\boldsymbol{\nu}_{\mathrm{v}}^f \triangleq [U_v, 0, 0]^T$ and $U_v \triangleq \|\boldsymbol{\nu}_{\mathrm{v}}^b\|$. The Flow frame is obtained as described in [22] as

$$\boldsymbol{R}_b^f \triangleq \boldsymbol{R}_{zy}(\alpha_v, -\beta_v), \tag{5}$$

where $\beta_v \triangleq \mathrm{atan2}(v_v, u_w)$ is the vehicle sideslip, $\alpha_v \triangleq \mathrm{atan2}(w_v, u_v)$ is the vehicle angle of attack and $u_w \triangleq \sqrt{u_v^2 + w_v^2}$. The vehicle kinematics can then be written as

$$\dot{\boldsymbol{p}}_{\mathrm{v}}^n = \boldsymbol{R}_{zy}(\theta_v, \psi_v)\boldsymbol{R}_{zy}(\alpha_v, -\beta_v)^T \boldsymbol{\nu}_{\mathrm{v}}^f. \tag{6}$$

The Euler angles of the f frame can be found using the procedure from [22] as

$$\varphi_f = \tan^{-1}\left[s(\beta_v)t(\gamma_v)\right], \tag{7}$$
$$\theta_f = \sin^{-1}\left[c(\beta_v)s(\gamma_v)\right], \tag{8}$$
$$\psi_f = \tan^{-1}\left(\tfrac{c(\gamma_v)s(\psi_v)c(\beta_v)+c(\psi_v)s(\beta_v)}{c(\gamma_v)s(\psi_v)c(\beta_v)+c(\psi_v)s(\beta_v)}\right), \tag{9}$$

where $\gamma_v \triangleq \theta_v - \alpha_v$. The Euler angle derivatives are

$$\begin{bmatrix}\dot{\varphi}_f \\ \dot{\theta}_f \\ \dot{\psi}_f\end{bmatrix} = \begin{bmatrix}1 & s(\varphi_f)t(\theta_f) & c(\varphi_f)t(\theta_f) \\ 0 & c(\varphi_f) & -s(\varphi_f) \\ 0 & s(\varphi_f)/c(\theta_f) & c(\varphi_f)/c(\theta_f)\end{bmatrix} \boldsymbol{\omega}_{nf}^f. \tag{10}$$

The angular velocity vector $\boldsymbol{\omega}_{nf}^f$ is found as [24]:

$$\boldsymbol{\omega}_{nf}^f = \boldsymbol{\omega}_{nb}^f + \boldsymbol{\omega}_{bf}^f = \boldsymbol{R}_{zy}(\alpha_v, -\beta_v)\boldsymbol{\omega}_{nb}^b + \boldsymbol{\omega}_{bf}^f, \tag{11}$$

where $\boldsymbol{\omega}_{nf}^f \triangleq [p_f, q_f, r_f]^T$, $\boldsymbol{\omega}_{nb}^b = [0, q_v, r_v]^T$ and $\boldsymbol{\omega}_{bf}^f$ can be found as $\boldsymbol{\omega}_{bf}^f = [-\dot{\beta}_v \sin(\alpha_v), -\dot{\alpha}_v, \dot{\beta}_v \cos(\alpha_v)]$.

Inserting for $\dot{\alpha}_v$ and $\dot{\beta}_v$ in (6)-(11) and rearranging gives

$$\begin{bmatrix}q_f \\ r_f\end{bmatrix} = \boldsymbol{A}_f \begin{bmatrix}q_v \\ r_v\end{bmatrix} + \boldsymbol{B}_f, \tag{12}$$

where

$$\boldsymbol{A}_f \triangleq \begin{bmatrix}c(\beta_v) - \frac{X_w u_v}{u_w^2} & -s(\beta_v)s(\alpha_v) \\ c(\alpha_v)\frac{X_w w_v v_v}{u_w U_v^2} & c(\alpha_v)\frac{u_w X_v + U_v^2}{U_v^2}\end{bmatrix}, \tag{13}$$

and

$$\boldsymbol{B}_f \triangleq \begin{bmatrix}c(\beta_v) - \frac{X_w u_v}{u_w^2} & v_v c(\alpha_v)\frac{Z_w s(\theta_v) w_v + Y_v u_w^2 + Y_w w_v^2}{u_w U_v^2}\end{bmatrix}^T. \tag{14}$$

It can be shown that $\boldsymbol{A}_f$ is nonsingular when the following assumption is met:

Assumption 4: The parameters X_v and X_w satisfy $X_v + u_v > 0$ and $-X_w + u_v > 0$.

This assumption ensures that a change in θ_v or ψ_v changes θ_f or ψ_f, respectively, and holds for most AUVs by design.

C. Analysis model

The $q_v - q_f$ and $r_v - r_f$ couplings in (12) complicate the analysis in Section VI. However, if the angles α_v and β_v can be assumed to be small, we can make the small angle approximations $c(\alpha_v) \approx 1$, $c(\beta_v) \approx 1$ and $s(\alpha_v)s(\beta_v) \approx 0$. Furthermore, $\beta_v \approx \mathrm{atan2}(v_v, u_v)$. Equation (12) can then be reduced to

$$q_f \approx q_v - \dot{\alpha}_v \tag{15}$$
$$r_f \approx r_v + \dot{\beta}_v. \tag{16}$$

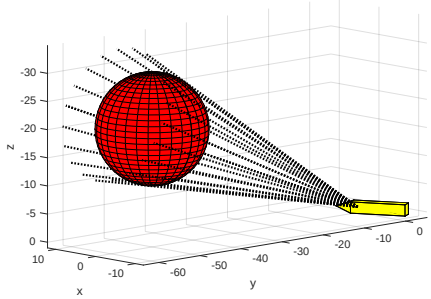

Fig. 1. A sample of rays (dotted black) from the vision cone from the vehicle (yellow) to the obstacle (red).

The sway and heave dynamics in (4d) and (4e) can then be rewritten in terms of q_f and r_f as

$$\dot{v}_v \approx \tfrac{u_v^2+v_v^2}{X_v u_v + u_v^2 + v_v^2}\left(X_v r_f + Y_v v_v\right), \tag{17}$$
$$\dot{w}_v \approx \tfrac{u_w^2}{u_w^2 - X_w u_v}\left(X_w q_f + Y_w w_v + Z_w \sin(\theta_v)\right). \tag{18}$$

The small angle assumption for α_v and β_v holds for vehicles where the hydrodynamic damping and rudder saturation ensures that turning rate is not too large, which is the case of most AUVs at maneuvering speed.

D. Obstacle model

The obstacle is modeled as a sphere with radius R_{o}. The obstacle position in the NED frame is denoted $\boldsymbol{p}_o^n$.

Remark 1: The algorithm can also be applied to non-spherical obstacles. However, an analysis containing such obstacles is beyond the scope of this paper.

E. Sensing model

We require that the vehicle is able to measure the distance d_{o} to the obstacle, as well as the angles to the edge of the obstacle. These angles define a three-dimensional vision cone $\mathcal{V}_{\mathrm{o}}$, which is illustrated in Fig. 1. For underwater vehicles, a sensor such as a forward looking sonar can give both d_{o} and $\mathcal{V}_{\mathrm{o}}$. The apex angle of $\mathcal{V}_{\mathrm{o}}$ is $2\gamma_{\mathrm{a}}$, where

$$\gamma_{\mathrm{a}} \triangleq \sin^{-1}\left(\frac{R_{\mathrm{o}}}{R_{\mathrm{o}} + d_{\mathrm{o}}}\right). \tag{19}$$

F. Control objectives

The control system and CA algorithm should make the vehicle come within an acceptance distance $d_{\mathrm{a}} \geq u_v / r_{v\max}$ of a target position $\boldsymbol{p}_{\mathrm{t}}^n$, i.e.

$$\exists t_{\mathrm{f}} \in [0, \infty) \quad \text{s.t.} \quad ||\boldsymbol{p}_{\mathrm{t}}^{n_v}(t_{\mathrm{f}})|| \leq d_{\mathrm{a}}, \tag{20}$$

where $\boldsymbol{p}_{\mathrm{t}}^{n_v} = \boldsymbol{p}_{\mathrm{t}}^n - \boldsymbol{p}_{\mathrm{v}}^n$ is the target position in n_v.

At all times, the distance d_{o} between the vehicle and the obstacle should satisfy

$$d_{\mathrm{o}}(t) \geq d_{\mathrm{safe}} > 0 \quad \forall t \in [t_0, t_f], \tag{21}$$

where the safety distance d_{safe} is a design parameter.

Many AUVs have pitch limitations to ensure that they do not move too fast towards the sea floor or the surface. For

this reason, we require that the control system bounds the pitch of the vehicle in the Flow frame as:

$$\theta_f(t) \in [\theta_{f\min}, \theta_{f\max}] \quad \forall t \in [t_0, t_f], \tag{22}$$

where $\theta_{f\min} \in (-\pi/2, 0)$ and $\theta_{f\max} \in (0, \pi/2)$ are constant design parameters.

IV. Control System

The control system can be either in guidance mode or in CA mode. In this section we describe the guidance laws used in guidance mode, as well as the controllers used to steer the Flow frame of the vehicle. The CA law is described in Section V, while the rule for switching between the two modes is given in Section V-B.

A. Flow frame control

To account for the underactuated dynamics, we will steer the direction of the vehicle's velocity vector, i.e. we will control $\dot{\theta}_f$ and $\dot{\psi}_f$. To this end, we use (12) to obtain

$$\begin{bmatrix} q_v \\ r_v \end{bmatrix} = \boldsymbol{A}_f^{-1} \left(\begin{bmatrix} q_f \\ r_f \end{bmatrix} - \boldsymbol{B}_f \right). \tag{23}$$

The Flow frame angular rates q_f and r_f are obtained as

$$q_f = c(\varphi_f)\dot{\theta}_f + c(\theta_f)s(\varphi_f)\dot{\psi}_f, \tag{24}$$

$$r_f = -s(\varphi_f)\dot{\theta}_f + c(\theta_f)c(\varphi_f)\dot{\psi}_f. \tag{25}$$

We design the controller to turn the vehicle velocity vector at a maximum rate towards the desired direction, to reach it as soon as possible, and we thus choose:

$$\dot{\theta}_f(\theta_\mathrm{d}) \triangleq \mathrm{sign}(\tilde{\theta}_f)\dot{\theta}_{f\max}, \tag{26a}$$

$$\dot{\psi}_f(\psi_\mathrm{d}) \triangleq \mathrm{sign}(\tilde{\psi}_f)\dot{\psi}_{f\max}, \tag{26b}$$

where $\tilde{\theta}_f \triangleq \theta_v - \theta_\mathrm{d}$ and $\tilde{\psi}_f \triangleq \psi_f - \psi_\mathrm{d}$. We define the error variables to lie in the interval $(-\pi, \pi]$ to ensure that the vehicle makes the shortest turn towards ψ_d and θ_d. The desired heading ψ_d and pitch θ_d are given in Section IV-B when the control system is in guidance mode, and in Section V when the control system is in CA mode.

B. Guidance laws

In guidance mode, a pure pursuit guidance law [25] is used to set θ_d and ψ_d. The desired heading ψ_dg in guidance mode is thus chosen as:

$$\psi_\mathrm{dg} \triangleq \Psi(\boldsymbol{p}_\mathrm{t}^{n_v}), \tag{27}$$

where Ψ is defined in (1).

The desired pitch θ_dg in guidance mode is saturated to ensure that control objective (22) is met:

$$\theta_\mathrm{dg} = \begin{cases} \theta_{f\max} & \Theta(\boldsymbol{p}_\mathrm{t}^{n_v}) > \theta_{f\max}, \\ \Theta(\boldsymbol{p}_\mathrm{t}^{n_v}) & \Theta(\boldsymbol{p}_\mathrm{t}^{n_v}) \in [\theta_{f\min}, \theta_{f\max}], \\ \theta_{f\min} & \Theta(\boldsymbol{p}_\mathrm{t}^{n_v}) < \theta_{f\min}, \end{cases} \tag{28}$$

where Θ is defined in (2). If $\Theta(\boldsymbol{p}_\mathrm{t}^{n_v}) \notin [\theta_{\min}, \theta_{\max}]$, the guidance law will drive the vehicle towards the target at maximum or minimum pitch, and then make the vehicle circle up or down until $||\boldsymbol{p}_\mathrm{t}^{n_v}(t_\mathrm{f})|| \leq d_\mathrm{a}$, and control objective (20) is met.

The desired velocity vector in guidance mode, $\boldsymbol{v}_\mathrm{dg}^{n_v}$, is then found from the guidance laws (27) and (28) as:

$$\boldsymbol{v}_\mathrm{dg}^{n_v} \triangleq \boldsymbol{R}_{zy}(\theta_\mathrm{dg}, \psi_\mathrm{dg}) \begin{bmatrix} U_v & 0 & 0 \end{bmatrix}^T. \tag{29}$$

V. Collision Avoidance Algorithm

In this section we define the CA algorithm and the rule for switching into and out of CA mode.

A. Algorithm definition

To get a cone from the vehicle to the obstacle where each ray has an avoidance angle $\alpha_\mathrm{o} \in [0, \pi/2)$ to the obstacle, the vision cone $\mathcal{V}_\mathrm{o}$ is extended to a cone $\mathcal{V}_\mathrm{e}$ with apex angle $2(\gamma_\mathrm{a} + \alpha_\mathrm{o}) := 2\gamma_\mathrm{e}$, as illustrated in Fig. 2.

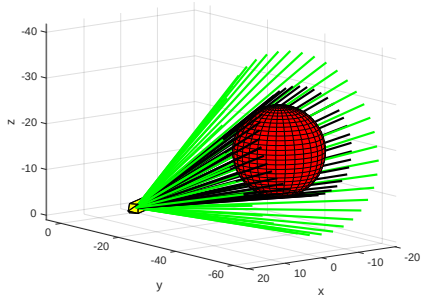

Fig. 2. The extended vision cone (green) from the vehicle to the obstacle

Remark 2: If the obstacle is non-spherical, each ray of the vision cone is rotated α_o radians in the direction normal to the obstacle surface.

To make the vehicle keep a constant avoidance angle to the obstacle, and thus avoid it, we will make the x-axis of the Flow frame point along a ray ρ of $\mathcal{V}_\mathrm{e}$. To this end, we will find the heading and pitch of each ray represented in the n_v frame. We do this by first representing the ray in a Body-fixed frame b_{vo}, where the x-axis points from the vehicle to the obstacle, and then perform a rotation to move from the b_{vo} to the n_v frame. The direction of any ray ρ in the n_v frame can then be parametrized as the unit vector $\boldsymbol{u}_\rho^{n_v}(\phi)$:

$$\boldsymbol{u}_\rho^{n_v}(\phi) = \boldsymbol{R}_{zyx}(\phi, \Theta(\boldsymbol{p}_o^{n_v}), \Psi(\boldsymbol{p}_o^{n_v}))\boldsymbol{R}_z(\gamma_\mathrm{e})\boldsymbol{u}_x, \tag{30}$$

where the parameter $\phi \in [0, 2\pi)$, $\boldsymbol{p}_o^{n_v}$ is the position of the obstacle in the n_v frame and $\boldsymbol{u}_x \triangleq [1, 0, 0]^T$. A vehicle, an obstacle and four rays of $\mathcal{V}_\mathrm{e}$ are shown in the b_{vo} frame in Fig. 3. The velocity direction required to follow a ray are defined by

$$\psi_{V_e}(\phi) \triangleq \Psi(\boldsymbol{u}_\rho^{n_v}(\phi)), \tag{31a}$$

$$\theta_{V_e}(\phi) \triangleq \Theta(\boldsymbol{u}_\rho^{n_v}(\phi)). \tag{31b}$$

Every direction along $\mathcal{V}_\mathrm{e}$ are suitable candidates for CA. This gives us flexibility, which we will utilize by choosing a direction that minimize a cost function C, defined as

$$C \triangleq \begin{cases} |\boldsymbol{e}_{V_e}|_\infty & \theta_{V_e} \in [\theta_{f\min}, \theta_{f\max}] \\ |\boldsymbol{e}_{V_e}|_\infty + 2\pi & \theta_{V_e} \notin [\theta_{f\min}, \theta_{f\max}], \end{cases} \tag{32}$$

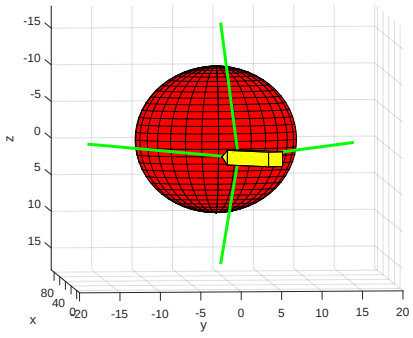

Fig. 3. Four rays of $\mathcal{V}_\mathrm{e}$ in the b_{vo} frame.

where $\boldsymbol{e}_{V_e}(\phi) \triangleq [\tilde{\psi}_{V_e}(\phi), \tilde{\theta}_{V_e}(\phi)]^T$ and

$$\tilde{\psi}_{V_e}(\phi) \triangleq \psi_v - \psi_{V_e}(\phi), \qquad \tilde{\psi}_{V_e}(\phi) \in (-\pi, \pi], \tag{33a}$$

$$\tilde{\theta}_{V_e}(\phi) \triangleq \theta_v - \theta_{V_e}(\phi), \qquad \tilde{\theta}_{V_e}(\phi) \in (-\pi, \pi]. \tag{33b}$$

Let $\phi_\mathrm{ca} \triangleq \arg\min_\phi C(\boldsymbol{e}_{V_e}(\phi))$. The desired heading and pitch angle in collision avoidance are

$$\langle \theta_\mathrm{dca}, \psi_\mathrm{dca} \rangle \triangleq \langle \theta_{V_e}(\phi_\mathrm{ca}), \psi_{V_e}(\phi_\mathrm{ca}) \rangle . \tag{34}$$

We thus make the vehicle use both its control inputs to avoid the obstacle, while we at the same time ensure that the pitch of the Flow frame stays within limit.

B. Switching rule

We define that the vehicle enters CA mode at a time t_1 if the obstacle is closer than or equal to a chosen range, d_switch, and the desired velocity vector $\boldsymbol{v}_\mathrm{dg}^{n_v}(t_1)$ (29) from the nominal guidance laws (27) and (28) is within the extended vision cone $\mathcal{V}_\mathrm{e}(t_1)$:

$$\boldsymbol{v}_\mathrm{dg}^{n_v}(t_1) \in \mathcal{V}_\mathrm{e}(t_1), \tag{35a}$$

$$d_\mathrm{o}(t_1) \leq d_\mathrm{switch} \in (d_\mathrm{safe}, d_\mathrm{sense}]. \tag{35b}$$

Nominal guidance towards the target will resume at a time t_2 when $\boldsymbol{v}_\mathrm{dg}^{n_v}(t_2)$ moves outside $\mathcal{V}_\mathrm{e}(t_2)$:

$$\boldsymbol{v}_\mathrm{dg}^{n_v}(t_2) \notin \mathcal{V}_\mathrm{e}(t_2). \tag{36}$$

VI. ANALYSIS

This section analyses the CA algorithm presented in Section V when applied to the vehicle model in Section III-A. The Flow frame f of the vehicle is steered using the controllers (26a) and (26b). When in guidance mode, the vehicle moves towards a target position $\boldsymbol{p}_\mathrm{t}^n$ using the guidance laws (27) and (28). When the vehicle encounters an obstacle, it switches into CA mode using the switching criterion in Section V-B, and avoids the obstacle by steering the direction of the velocity vector according to (34).

A. Sway and heave bounds

In order to bound U_v, q_f and r_f, we need to bound the sway and heave velocities. This is done by using the analysis model (15)-(18) in the following lemma:

Lemma 1: Let the sway and heave velocities be modeled by (17) and (18), and let $|q_f| \leq q_{f\max} > 0$ and $|r_f| \leq r_{f\max} > 0$. Furthermore, let $v_v(0) \leq v_{f\max}$ and $w_v(0) \leq w_{f\max}$, where

$$v_{f\max} = \frac{|X_v|}{|Y_v|} r_{f\max}, \tag{37}$$

$$w_{f\max} = \frac{|X_w|}{|Y_w|} q_{f\max} + \frac{|Z_w|}{|Y_w|}. \tag{38}$$

Then, for all $t \geq 0$, we have that $v_v(t) \leq v_{f\max}$ and $w_v(t) \leq w_{f\max}$.

Proof: Consider the Lyapunov function candidate $V(w_v) = 0.5 w_v^2$ of (18). The time derivative of V is upper bounded by

$$\dot{V} \leq \frac{u_w^2}{u_w^2 - X_w u_v} \left(|X_w||w_v| q_{f\max} + |Y_w||w_v|^2 + |Z_w| \right). \tag{39}$$

Let the set Ω_V be defined as

$$\Omega_V \triangleq \{ w_v \in \mathbb{R} \mid V \leq \tfrac{1}{2} w_{f\max}^2 \}, \tag{40}$$

which is a level set of V with $w_v = w_{f\max}$ on the boundary. On the boundary of Ω_V, the definition of $w_{f\max}$ (38) ensures that $\dot{V} \leq 0$. Hence, any solution of w_v starting in Ω_V cannot leave it, which concludes the proof for $w_{f\max}$. The proof for $v_{f\max}$ is equivalent. ■

B. Flow frame angular rates

To find values of $q_{f\max}$ and $r_{f\max}$ which do not violate Assumption 2, we use (15)-(16) to obtain the inequalities

$$\frac{(u_v^2 + w_{f\max}^2) q_{f\max} + |Y_w| u_v w_{f\max} + u_v |Z_w|}{u_v (u_v - X_w)} \leq q_{v\max}, \tag{41}$$

$$\frac{(u_v^2 + v_{f\max}^2) r_{f\max} + |Y_v| u_v v_{f\max}}{u_v (X_w + u_v)} \leq r_{v\max}. \tag{42}$$

Assumption 4 ensures that these inequalities have a positive solution for $q_{f\max}$ and $r_{f\max}$, which can be found graphically by inserting for $v_{f\max}$ (37) and $w_{f\max}$ (38). From (24) and (25) we see that the bounds on q_f and r_f are upheld if $\dot{\theta}_{f\max} \leq \min\{q_f, r_f\}$ and $\dot{\psi}_{f\max} \leq \min\{q_f, r_f\}$.

C. Safety distance

To ensure that the vehicle stays at least a minimum safety distance d_safe away from the obstacle during the CA maneuver, the avoidance angle α_o needs to be lower bounded as shown in Lemma 2.

Lemma 2: If

$$\alpha_\mathrm{o} \geq \cos^{-1}\left(\frac{R_\mathrm{o}}{R_\mathrm{o} + d_\mathrm{safe}} \right), \tag{43}$$

the initial obstacle distance $d_\mathrm{o}(t_0) \geq d_\mathrm{safe}$, and the vehicle follows the CA law (34), then $d_\mathrm{o}(t) \geq d_\mathrm{safe}$ for all $t \geq t_0$.

Proof: When the vehicle's velocity vector points along a ray of the extended vision cone, $\dot{d}_\mathrm{o}$ can be found as:

$$\dot{d}_\mathrm{o} = -U_v \cos(\gamma_\mathrm{a}(t) + \alpha_\mathrm{o}). \tag{44}$$

When $\gamma_{\text{a}}(t) = \pi/2 - \alpha_{\text{o}}$, $\dot{d}_{\text{o}} = 0$. This occurs when

$$d_{\text{o}}(t) = d_{\text{omin}} \triangleq \frac{R_{\text{o}}}{\cos(\alpha_{\text{o}})} - R_{\text{o}}. \tag{45}$$

Furthermore, when $d_{\text{o}}(t) < d_{\text{omin}}$, $\dot{d}_{\text{o}}(t) > 0$, while when $d_{\text{o}}(t) > d_{\text{omin}}$, $\dot{d}_{\text{o}}(t) < 0$. It follows that if $d_{\text{safe}} = d_{\text{omin}}$ and $d_{\text{o}}(t_0) \geq d_{\text{safe}}$, then a vehicle following (34) will not get closer than d_{safe} to the obstacle. ■

D. Safe avoidance

We now show that if the vehicle velocity is aligned with the extended vision cone at some time t_2, then the vehicle is guaranteed to be safe from collision as long as it is in CA mode.

Lemma 3: Consider a vehicle modeled by (4) and governed by the controllers (26), the guidance laws (27) and (28) and the CA law (34). Let there exist a time t_2 when the vehicle is in CA mode, $d_{\text{o}}(t_2) \geq d_{\text{safe}}$, $\psi_f(t_2) = \psi_{\text{dca}}$ and $\theta_f(t_2) = \theta_{\text{dca}}$. Finally, let there be a time $t_3 > t_2$ at which the vehicle exits CA mode. Then, the distance to the obstacle satisfies

$$d_{\text{o}}(t) \geq d_{\text{safe}} \quad \forall t \in [t_2, t_3]. \tag{46}$$

Proof: Fig. 4 shows a plane P_ρ containing the ray ρ the vehicle is aligned with at time t_2, the vehicle and the obstacle center. Without loss of generality, let the x-axis of the Flow frame, denoted x^f in the figure, lie in P_ρ. The angle from the x-axis of P_ρ to b is denoted ψ_ρ, while the angle to ρ is denoted γ_ρ, which can be decomposed as

$$\gamma_\rho = \gamma_{\text{o}} + \gamma_{\text{a}} + \alpha_0. \tag{47}$$

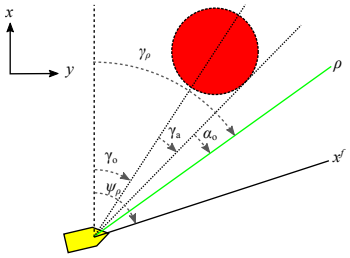

Fig. 4. The vehicle and the obstacle in the plane P_ρ containing the ray ρ and the obstacle center.

It follows from (47) that

$$\dot{\gamma}_\rho = \dot{\gamma}_{\text{o}} + \dot{\gamma}_{\text{a}}. \tag{48}$$

The angular velocity of γ_{o} can be found geometrically as

$$\dot{\gamma}_{\text{o}} = -\frac{U_v}{R_{\text{o}}+d_{\text{o}}} \sin(\psi_\rho - \gamma_{\text{o}}). \tag{49}$$

while

$$\dot{\gamma}_{\text{a}} = -\dot{d}_{\text{o}} \frac{R_{\text{o}}}{(R_{\text{o}}+d_{\text{o}})\sqrt{(R_{\text{o}}+d_{\text{o}})^2 - R_{\text{o}}^2}}, \tag{50}$$

where $\dot{d}_{\text{o}} = -U_v \cos(\psi_\rho - \gamma_{\text{o}})$.

We define the error variable $\tilde{\psi}_\rho \triangleq \psi_\rho - \gamma_\rho$. The dynamics of $\tilde{\psi}_\rho$ are obtained from (49) and (50) as

$$\dot{\tilde{\psi}}_\rho = \dot{\psi}_\rho - \dot{\gamma}_\rho = \dot{\psi}_\rho + \frac{U_v \sin(\tilde{\psi}_\rho + \alpha_0)}{\sqrt{(R_{\text{o}}+d_{\text{o}})^2 - R_{\text{o}}^2}}, \tag{51}$$

where $\dot{\psi}_\rho$ is set by the controllers in (26). When $\tilde{\psi}_\rho = 0$,

$$\dot{\tilde{\psi}}_\rho = \dot{\psi}_\rho + \frac{U_v \sin(\alpha_0)}{\sqrt{(R_{\text{o}}+d_{\text{o}})^2 - R_{\text{o}}^2}}. \tag{52}$$

The rightmost term is positive since $\alpha_0 \in (0, \frac{\pi}{2})$, while $\dot{\psi}_\rho \in [-\dot{\psi}_{\rho\text{max}}, \dot{\psi}_{\rho\text{max}}]$, where $\dot{\psi}_{\rho\text{max}} \triangleq \sqrt{r_{f\text{max}}^2 + q_{f\text{max}}^2}$. If $\dot{\gamma}_\rho > \dot{\psi}_{\rho\text{max}}$, it follows from (52) that $\dot{\tilde{\psi}}_\rho > 0$. Hence, the vehicle direction will drift away from the extended vision cone $\mathcal{V}_{\text{e}}$ and the vehicle will move away from the obstacle by Lemma 2. This can be seen from Figure 4, where it is clear that a direction outside of ρ will lead the vehicle further away from the obstacle than following ρ.

If the desired direction from minimizing the cost function $C(\boldsymbol{e}_{V_e}(\phi))$ in (32) makes the vehicle move away from the plane P_ρ, the vehicle direction will still glide away from $\mathcal{V}_{\text{e}}$ since the obstacle is convex. Hence, as long as there is a time t_2 when the vehicle is aligned with a ray of $\mathcal{V}_{\text{e}}$, the vehicle distance is guaranteed to be greater than d_{safe} while the vehicle is in CA mode. ■

E. Safe navigation

In this section we prove that the vehicle will safely traverse an environment containing an obstacle and reach the target position. This is the main theorem of the paper. Before we state the theorem, we make the assumptions that the vehicle is able to start safely, and that the obstacle does not cover the target.

Assumption 5:

$$\theta_f(t_0) \in [\theta_{f\text{min}}, \theta_{f\text{max}}]. \tag{53}$$

Assumption 6:

$$d_{\text{o}}(t_0) > d_{\text{switch}}. \tag{54}$$

Assumption 7: The distance $d_{\text{o,t}}$ from the obstacle to the target position $\boldsymbol{p}_{\text{t}}^n$ satisfies

$$d_{\text{o,t}} > \frac{R_{\text{o}}}{\cos(\alpha_{\text{o}})} - R_{\text{o}}. \tag{55}$$

Theorem 1: Let Assumptions 1-7 hold, the avoidance angle α_{o} satisfy

$$\alpha_{\text{o}} \in \left[\cos^{-1}\left(\frac{R_{\text{o}}}{R_{\text{o}}+d_{\text{safe}}}\right), \frac{\pi}{2}\right), \tag{56}$$

and the switching distance satisfy

$$d_{\text{switch}} \geq U_{v\text{max}}/\dot{\psi}_{f\text{max}} + d_{\text{safe}}. \tag{57}$$

Furthermore, let the vehicle kinematics be be modeled by (4a)-(4c), the sway and heave dynamics modeled by (17)-(18), and the vehicle governed by the controllers (26), the guidance laws (27) and (28) and the CA law (34). Then, there exists a time $t_{\text{f}} \geq t_0$ such that

$$||\boldsymbol{p}_{\text{t}}^{n_v}(t_{\text{f}})|| \leq d_{\text{a}}. \tag{58}$$

Moreover,

$$d_{\text{o}}(t) \geq d_{\text{safe}} \quad \forall t \in [t_0, t_f], \tag{59}$$

and

$$\theta_f(t) \in [\theta_{f\text{min}}, \theta_{f\text{max}}] \quad \forall t \in [t_0, t_f]. \tag{60}$$

Hence, the control objectives (20), (21) and (22) are met.

Proof: Consider a time $t_1 \geq t_0$, at which the vehicle enters CA mode in accordance with (35). The vehicle then chooses a direction which minimizes the cost function C, and starts turning towards this direction.

The turning radius of the vehicle is largest when the pitch limitations forces it to only use the horizontal control intput. The heading change required to avoid the obstacle is then upper bounded by $\pi/2$ rad, which gives a turning radius of $U_{v\max}/\dot{\psi}_{f\max}$, where $U_{v\max} \triangleq \|[u_v, v_{f\max}, w_{f\max}]^T\|$. Hence, the vehicle will move a maximum distance of $U_{v\max}/\dot{\psi}_{f\max}$ towards the obstacle before reaching the extended vision cone $\mathcal{V}_\mathrm{e}$. The minimum switching distance given by (57) thus ensures that there is a time $t_2 > t_1$ at which the vehicle is aligned with a ray of $\mathcal{V}_\mathrm{e}$, and that

$$d_\mathrm{o}(t) \geq d_\mathrm{safe} \quad \forall t \in [t_0, t_2]. \tag{61}$$

At time t_2, the conditions of Lemma 3 are met. Hence, the obstacle distance will not be less than d_safe until a time $t_3 > t_2$, when the direction towards the target comes outside $\mathcal{V}_\mathrm{e}$. By the switching rule in Section V-B, the control system now enters guidance mode. Lemma 2 implies that $d_\mathrm{o} \geq d_\mathrm{safe}$ when the vehicle velocity vector points outside $\mathcal{V}_\mathrm{e}$. Hence it is ensured that condition (59) is fulfilled.

The guidance laws in (27) and (28) steers the vehicle towards the target at maximum turning rate. Hence, it is ensured that there exist a finite time t_f when $||\boldsymbol{p}_\mathrm{t}^{n_v}(t_\mathrm{f})|| \leq d_\mathrm{a}$, fulfilling condition (58).

While the definition of C ensures that $\theta_\mathrm{dca} \in [\theta_{f\min}, \theta_{f\max}]$, the definition of the pitch guidance law (28) ensures that $\theta_\mathrm{dg} \in [\theta_{f\min}, \theta_{f\max}]$. Assumption 5 and the pitch control law (26a) then ensure that condition (60) is fulfilled. ■

Remark 3: This proof also holds for a scenario with multiple obstacles, under the condition that the separation distance is at least $2d_\mathrm{switch}$.

VII. Simulations

In this section, we present numerical simulations of the HUGIN AUV [26] to validate the analysis in Section VI. The simulation parameters are shown in Table I.

TABLE I
SIMULATION PARAMETERS

$r_{v\max}$	$1\,\mathrm{rad/s}$	$\theta_{f\min}$	$-35\,^\circ$
$q_{v\max}$	$1.5\,\mathrm{rad/s}$	$\theta_{f\max}$	$35\,^\circ$
u_v	$2\,\mathrm{m/s}$	$\boldsymbol{p}_\mathrm{v}^n(t_0)$	$[0,0,0]^T$ (m)
R_o	$20\,\mathrm{m}$	$\boldsymbol{p}_\mathrm{t}^n(t_0)$	$[150,0,0]^T$ (m)
d_safe	$5\,\mathrm{m}$	d_a	$20\,\mathrm{m}$

The Flow frame maximum angular rates are set to $q_{f\max} = r_{f\max} = \dot{\theta}_{f\max} = \dot{\psi}_{f\max} = 0.11\,\mathrm{rad/s}$. Using Lemma 1 we find that $v_{f\max} = 0.16$ and $w_{f\max} = 0.24$, which gives $\alpha_v \leq 0.12\,\mathrm{rad}$ and $\beta_v \leq 0.08\,\mathrm{rad}$, which satisfies the small angle assumption used in the analysis model. Note, however, that the more precise model for sway and heave dynamics in (4d)-(4e) is used in the simulation.

The avoidance angle α_o was set using (56) to $36.9\,^\circ$, while the switching distance was set using (57) to $d_\mathrm{switch} = 23.4\,\mathrm{m}$.

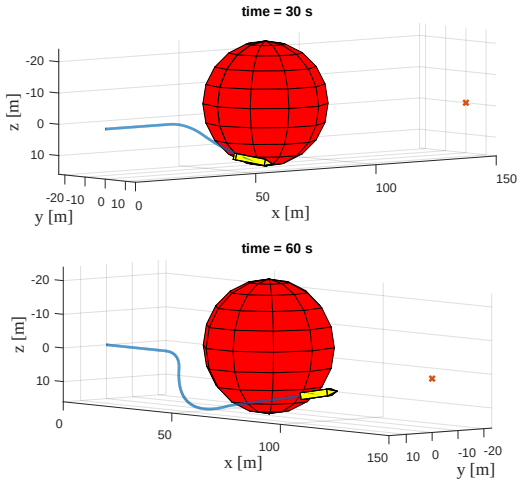

Fig. 5. A scenario where $y_\mathrm{o,sim} = -4\,\mathrm{m}$ and $z_\mathrm{o,sim}$ $-4\,\mathrm{m}$. The vehicle is the yellow polyhedron, and the obstacle is the red sphere. The blue line is the vehicle trajectory, while the target is marked by an 'X'.

The obstacle position was set to $\boldsymbol{p}_o^n = [70, y_\mathrm{o,sim}, z_\mathrm{o,sim}]^T$ (m), where $y_\mathrm{o,sim}$ and $z_\mathrm{o,sim}$ increased incrementally from $-20\,\mathrm{m}$ to $20\,\mathrm{m}$ in steps of $2\,\mathrm{m}$ for each run. The results are summarized in Table II.

TABLE II
SIMULATION RESULTS

Min d_omin	$5.8\,\mathrm{m}$	Max d_omin	$12.1\,\mathrm{m}$
Min $t_\mathrm{f} - t_0$	$66.2\,\mathrm{s}$	Max $t_\mathrm{f} - t_0$	$73.5\,\mathrm{s}$
Max q_v	$0.76\,\mathrm{rad/s}$	Max r_v	$0.56\,\mathrm{rad/s}$

Here, $d_\mathrm{o,min}$ denotes the minimum obstacle distance during a simulation.

The results in Table II verify the results of Theorem 1 in that the vehicle always reaches the target and that the safety distance is never violated. Furthermore, the bounds on q_v and r_v are not exceeded, and the maximum error in the angular rates of the analysis model is small.

An example scenario is shown in Fig. 5, where $y_\mathrm{o,sim} = z_\mathrm{o,sim} = -4\,\mathrm{m}$. Thus, the cost function C makes the vehicle move down and to the right. The pitch of the Flow frame is limited by $\theta_{f\min}$ and $\theta_{f\max}$ during the simulation, which makes the vehicle employ slightly more horizontal movement than vertical movement when circumventing the obstacle. When the line of sight to the target comes outside $\mathcal{V}_\mathrm{e}$, the vehicle exits CA mode and continues under nominal guidance towards the target position.

The magnitude of the error resulting from using the analysis model in (15)-(16) to obtain q_v and r_v are shown in Figure 6. The error remains small throughout the simulation, justifying the small angle approximation employed to find the bounds on $q_{f\max}$ and $r_{f\max}$ in Section VI-B.

VIII. Conclusions and Future Work

This paper has presented a 3D reactive collision avoidance algorithm for vehicles with underactuated dynamics in sway

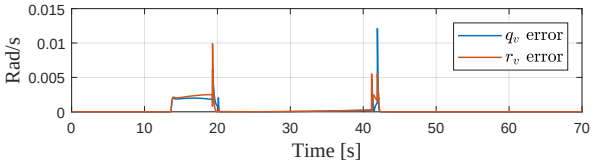

Fig. 6. The error resulting from using the analysis model to find q_v and r_v.

and heave. The underactuated states are accounted for by steering the direction of the vehicle's velocity vector, rather than the vehicle's attitude. To achieve this, a transformation between the angular rates of the vehicle's attitude and the angular rates of the vehicle's velocity has been derived. Furthermore, it is shown how the latter can be constrained in order to ensure that any given bounds on attitude rates are not exceeded.

During the collision avoidance maneuver, the algorithm makes the vehicle keep a constant avoidance angle to the obstacle. Safety bounds on the pitch of the velocity vector are incorporated in the algorithm. Such bounds are commonly seen in real life scenarios involving, for example, fixed wing aircraft or AUVs. Furthermore, an optimization criterion is presented in order to chose the best safe velocity direction in some sense. We have chosen the safe velocity vector which minimizes the maximum change in the heading and pitch of the vehicle's velocity vector. However, the criterion is easily extendible to such features as different weights on horizontal and vertical turning maneuvers, or compliance with rules of the road.

The main theorem of the paper gives explicit expressions for the minimum switching distance and avoidance angle required in order to ensure that the vehicle never comes within the a safety distance from the obstacle. Furthermore, it is shown how the underactuated dynamics can be bounded when applying the controllers derived in this paper. The results are verified by several simulations.

The analysis in this paper holds for scenarios with multiple obstacles, provided that the inter-obstacle distance is large enough to let the vehicle consider one obstacle at a time. In a scenario with dense clusters of obstacles, the different extended vision cones will have to be merged. This is a topic for further work, as is the inclusion of moving obstacles.

REFERENCES

[1] K. Y. Pettersen and O. Egeland, "Exponential stabilization of an underactuated surface vessel," in *Proc. 35th IEEE Conference on Decision and Control*, (Kobe, Japan), pp. 1391–1396, 1991.

[2] T. Statheros, G. Howells, and K. M. Maier, "Autonomous Ship Collision Avoidance Navigation Concepts, Technologies and Techniques," *Journal of Navigation*, vol. 61, no. 01, pp. 129–142, 2008.

[3] C. Tam, R. Bucknall, and A. Greig, "Review of Collision Avoidance and Path Planning Methods for Ships in Close Range Encounters," *The Journal of Navigation*, vol. 62, no. 2009, pp. 455–476, 2009.

[4] M. Hoy, A. S. Matveev, and A. V. Savkin, "Algorithms for collision-free navigation of mobile robots in complex cluttered environments: a survey," *Robotica*, vol. 33, no. 03, pp. 463–497, 2014.

[5] O. Khatib, "Real-time obstacle avoidance for manipulators and mobile robots," *The International Journal of Robotics Research*, vol. 5, no. 1, pp. 90–98, 1986.

[6] G. Roussos, D. V. Dimarogonas, and K. J. Kyriakopoulos, "3D navigation and collision avoidance for nonholonomic aircraft-like vehicles," *International Journal of Adaptive Control and Signal Processing*, vol. 24, pp. 900–920, 2010.

[7] D. Panagou, "Motion planning and collision avoidance using navigation vector fields," in *Proc. IEEE International Conference on Robotics & Automation (ICRA)*, (Hong Kong, China), pp. 2513–2518, 2014.

[8] D. Fox, W. Burgard, and S. Thrun, "The dynamic window approach to collision avoidance," *IEEE Robotics and Automation Magazine*, vol. 4, no. 1, pp. 23–33, 1997.

[9] B. O. H. Eriksen, M. Breivik, K. Y. Pettersen, and M. S. Wiig, "A modified dynamic window algorithm for horizontal collision avoidance for AUVs," in *Proc. 2016 IEEE Conference on Control Applications (CCA)*, (Buenos Aires, Brazil), pp. 499–506, 2016.

[10] P. Fiorini and Z. Shiller, "Motion planning in dynamic environments using velocity obstacles," *The International Journal of Robotics Research*, vol. 17, no. 7, pp. 760–772, 1998.

[11] A. Chakravarthy and D. Ghose, "Obstacle avoidance in a dynamic environment: A collision cone approach," *IEEE Transactions on Systems, Man, and Cybernetics Part A:Systems and Humans.*, vol. 28, no. 5, pp. 562–574, 1998.

[12] D. Wilkie, J. Van Den Berg, and D. Manocha, "Generalized velocity obstacles," in *Proc. IEEE/RSJ International Conference on Intelligent Robots and Systems,*, (St. Louis, MA, USA), pp. 5573–5578, 2009.

[13] J. van den Berg, J. Snape, S. J. Guy, and D. Manocha, "Reciprocal collision avoidance with acceleration-velocity obstacles," in *Proc. IEEE International Conference on Robotics and Automation (ICRA 2011)*, (Shanghai, China), pp. 3475–3482, 2011.

[14] Y. I. Jenie, E.-J. Van Kampen, C. C. de Visser, J. Ellerbroek, and J. M. Hoekstra, "Three-Dimensional Velocity Obstacle Method for UAV Deconflicting Maneuvers," in *Proc. AIAA Guidance, Navigation, and Control Conference*, (Kissimmee, FL, USA), 2015.

[15] Y. I. Jenie, E.-J. van Kampen, C. C. de Visser, J. Ellerbroek, and J. M. Hoekstra, "Three-Dimensional Velocity Obstacle Method for Uncoordinated Avoidance Maneuvers of Unmanned Aerial Vehicles," *Journal of Guidance, Control, and Dynamics*, vol. 39, no. 10, pp. 2312–2323, 2016.

[16] E. Lalish and K. A. Morgansen, "Distributed reactive collision avoidance," *Autonomous Robots*, vol. 32, no. 3, pp. 207–226, 2012.

[17] A. V. Savkin and C. Wang, "A simple biologically inspired algorithm for collision-free navigation of a unicycle-like robot in dynamic environments with moving obstacles," *Robotica*, vol. 31, no. 6, pp. 993–1001, 2013.

[18] C. Wang, A. V. Savkin, and M. Garrett, "A Strategy for Safe 3D Navigation of Non-Holonomic Under-Actuated Robots among Moving Obstacles," *Robotica*, vol. 36, no. 2, pp. 275–927, 2018.

[19] M. S. Wiig, K. Y. Pettersen, and A. V. Savkin, "A reactive collision avoidance algorithm for nonholonomic vehicles," in *Proc. 1st IEEE Conference on Control Technology and Applications*, (Kona, HI, USA), 2017.

[20] M. S. Wiig, K. Y. Pettersen, and T. R. Krogstad, "A reactive collision avoidance algorithm for vehicles with underactuated dynamics," in *Proc. 56th IEEE Conference on Control Technology and Applications*, (Melbourne, Australia), 2017.

[21] M. S. Wiig, K. Y. Pettersen, and T. R. Krogstad, "A 3D reactive collision avoidance algorithm for nonholonomic vehicles," in *2nd. IEEE Conference on Control Technology and Applications.*, 2018. Submitted, available at https://www.dropbox.com/sh/ze6mz1785agkhbw/AACfWMDfXeNil3ru1L29INILa?dl=0.

[22] T. I. Fossen, *Handbook of marine craft hydrodynamics and motion control*. John Wiley & Sons, 2011.

[23] M. S. Wiig, W. Caharija, T. R. Krogstad, and K. Y. Pettersen, "Integral Line-of-Sight Guidance of Underwater Vehicles Without Neutral Buoyancy," in *Proc. 10th IFAC Confererence on Control Applications in Marine Systems*, (Trondheim, Norway), pp. 590–597, 2016.

[24] E. Borhaug and K. Y. Pettersen, "LOS path following for underactuated underwater vehicle," in *Proc. 7th IFAC Conference on Manoeuvring and Control of Marine Craft*, (Lisbon, Portugal), 2006.

[25] M. Breivik and T. I. Fossen, "Guidance laws for planar motion control," in *Proc. IEEE Conference on Decision and Control*, (Cancun, Mexico), pp. 570–577, 2008.

[26] P. E. Hagen, N. Storkersen, K. Vestgard, and P. Kartvedt, "The HUGIN 1000 autonomous underwater vehicle for military applications," in *Proc. Oceans 2003*, (San Diego, CA, USA), pp. 1141–1145, 2003.